Dalton Transactions

PAPER

View Article Online
View Journal | View Issue

Cite this: *Dalton Trans.*, 2014, **43**, 13637

Selective complexation of α-amino acids and simple peptides *via* their carboxylate groups†

Roland Schnitter, Daniel Gallego and Berthold Kersting*

Received 2nd July 2014,
Accepted 29th July 2014

DOI: 10.1039/c4dt02007c

www.rsc.org/dalton

The complexation of anions of selected α-amino acids (alanine, valine, proline, tyrosine) and small peptides (L-alanyl-L-alanine, L-alanyl-L-alanyl-L-alanine, and L-alanyl-L-alanyl-L-alanyl-L-alanine) by the dinuclear nickel(II) complex $[LNi_2(\mu\text{-}Cl)]^+$ (**1**), where $(L)^{2-}$ represents a 24-membered binucleating hexamine-dithiophenolato ligand, has been investigated. The following complexes were prepared, isolated as perchlorate or tetraphenylborate salts, and characterized by UV/Vis, IR, and CD spectroscopy: $[LNi_2(\mu\text{-L-alaninato})]^+$ (**2**), $[LNi_2(\mu\text{-L-valinato})]^+$ (**3**), $[LNi_2(\mu\text{-L-prolinato})]^+$ (**4**), $[LNi_2(\mu\text{-L-tyrosinato})]^+$ (**5a**), $[LNi_2(\mu\text{-D-tyrosinato})]^+$ (**5b**), $[LNi_2(\mu\text{-L,D-tyrosinato})]^+$ (**5c**), $[LNi_2(\mu\text{-L-alanyl-L-alaninato})]^+$ (**6**), $[LNi_2(\mu\text{-(L-alanyl)}_2\text{-L-alaninato})]^+$ (**7**), $[LNi_2(\mu\text{-(L-alanyl)}_3\text{-L-alaninato})]^+$ (**8**). Compounds **4**, **5a** and **6** were additionally identified by X-ray crystallography. In contrast to unsupported amino carboxylate complexes which typically contain five membered NO chelate rings, the $[LNi_2]^{2+}$ fragment selectively binds the α-amino acids and peptides *via* $\mu_{1,3}$-bridging carboxylato groups. Coordination of the carboxylato coligands in this way confers dissymmetry on the complexes. The CD spectra of the *syn,syn*-bridged structures are significantly different from those of the NO chelates, and can distinguish between the two coordination modes. The encapsulation of the peptides increases their solubility in the solvent system MeOH–MeCN by up to two orders of magnitude. This is discussed in terms of the absence of intermolecular hydrogen bonding interactions as indicated in the X-ray structure of **6**.

Introduction

It is well-known that nickel(II) forms stable complexes with a range of amino acids and peptides, and that some of these complexes are of biological and technological relevance. The uptake and transport of nickel in plants, for example, is accomplished mainly by monomeric amino acids,[1,2] while nickel transport in blood plasma is governed by oligopeptides.[3] The molecular mechanisms of nickel toxicity appear to be associated with complexation of peptides as well.[4] For instance, the N terminal XZH motif in serum albumin, which mediates transport of nickel in blood plasma, has been identified as the primary nickel binding site.[5] Nickel may also bind to the octarepeat region of prion proteins and amyloid-β.[6] Moreover, the affinity of nickel for the amino acid histidine is also of importance in the purification of recombinant proteins utilizing the N-terminal hexa-histidyl tag. As a consequence much interest has arisen in the coordination chemistry of nickel with amino acids and peptides,[7] and a number of reviews on this topic exist.[8] There is also large interest in the coordination chemistry of organometallic nickel compounds with amino acids and peptides.[9]

Most of the amino acids invariably bind to nickel(II) *via* the carboxylate-O and the amino-N donor atom, thereby forming a thermodynamically stable, five-membered chelate ring.[10] The glycinato complex $[Ni(gly)_3]^-$ is a typical example.[11] The NO chelate prevails also in a number of mixed ligand complexes,[12] and in the case of amino acids with side chain donors.[13–15] The O,O-(carboxylate) coordination mode with a dangling NH_2 (or protonated-NH_3^+) function has been observed far less frequently.[16] It occurs in some mono- and polynuclear lanthanide complexes,[17,18] and in some dinuclear 4d and 5d metal complexes.[19,20] Carboxylate-O coordination has also been observed in ternary metal complexes designed to differentiate between L and D amino acids.[21] Here, the carboxylate coordination is enforced by an appended crown-ether moiety which binds the NH_3^+ group *via* three strong NH···O hydrogen-bonding interactions.[22]

The coordination modes of di-, tri-, and tetrapeptide ligands are more diverse as one might expect. In the absence of supporting ligands, the peptides generally act as chelate ligands, with a terminal N, one or more deprotonated amide

Institut für Anorganische Chemie, Universität Leipzig, Johannisallee 29, D-04103 Leipzig, Germany. E-mail: b.kersting@uni-leipzig.de; Fax: +49(0)341-97-36199

†Electronic supplementary information (ESI) available. CCDC 982688, 982689 and 1011258. For ESI and crystallographic data in CIF or other electronic format see DOI: 10.1039/c4dt02007c

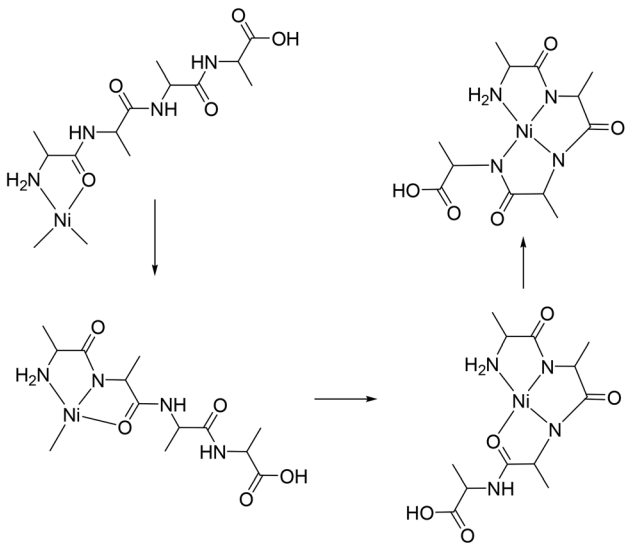

Scheme 1 Complexation of Ni(II) by tetrapeptides.[24]

ions and/or the carboxylato group.[8,12] In the case of simple oligopeptides with non-coordinating side chains, complex formation with Ni(II) starts at the N-terminal end and proceeds as shown in Scheme 1.[23] The affinity of Ni for dipeptide esters can be utilized in the metal-ion templated synthesis of cyclotetrapeptides.[24]

Our group is interested in the coordination chemistry of dinuclear nickel complexes supported by the hexaaza-dithiophenolato macrocycle $(L)^{2-}$ (Fig. 1).[25] The macrocycle supports mixed-ligand complexes of the type $[LNi_2(L')]^+$ with a capsular, cleft-like structure reminiscent of the "cone" conformation of the calixarenes.[26] It has been established that the binding cavity influences many properties of the complexes, particularly complex stability[27,28] and reactivity.[29–31] Several $[LNi_2(\mu\text{-}L')]^+$ complexes with carboxylato groups (RCO_2^-) as a coligand (L′) have been reported and crystallographically characterized.[32] Besides dinuclear $[LNi_2(\mu\text{-}O_2CR)]^+$ structures of aliphatic and aromatic carboxylates,[25] we have also reported higher-nuclearity complexes of the type $[(LNi_2)_2(\mu\text{-}O_2C\text{-}R\text{-}CO_2)]^{2+}$, in which pairs of bioctahedral $[LNi_2]^{2+}$ units are joined by a dicarboxylato dianion.[33] In some of these complexes, the carboxylate ions adopt unusual conformations attributable to confinement as for instance in $[LNi_2(\mu\text{-}3,4\text{-}$dimethyl-6-phenylcyclohex-3-enecarboxylate)], where the phenyl ring and the carboxylate group both assume axial positions with respect to the cyclohexene ring.[34,35]

The high carboxylate ion affinity of the $[LNi_2]^{2+}$ fragment suggested that a selective coordination of amino acids and simple peptides is possible. On these grounds we synthesized and characterized a series of new $[LNi_2(\mu\text{-}L')]^+$ complexes bearing selected α-amino acids and small peptides as coligands (L′). Their preparation, spectroscopic properties (IR, UV/Vis, CD) and structures are reported herein.

Results and discussion

Synthesis of complexes

The α-amino carboxylato complexes **2–5** were synthesized by ligand substitution reactions from the chlorido-bridged complex **1**, as it is depicted in Scheme 2. Treatment of complex **1** with a suspension of the respective α-amino acid in MeOH–MeCN in the presence of NEt_3 resulted in the formation of a pale green solution, from which the corresponding $[LNi_2(\text{aminocarboxylato})]^+$ species could be isolated as a pale-green perchlorate salt in 56–94% isolated yields. Salt metathesis of the perchlorate salts **2–5** with $NaBPh_4$ in methanol provided the corresponding tetraphenylborate salts **2′–5′**. The ESI mass spectra with a peak for the $[LNi_2(\mu\text{-aminocarboxylato})]^+$ cation and elemental analysis confirmed their constitution in each case (Table 1).

All compounds are air stable in solution as well as in solid state. The perchlorate salts exhibit good solubility in polar aprotic solvents such as MeCN, CH_2Cl_2 and acetone (5–10 mg ml^{-1}). They are less soluble in alcohol and virtually insoluble in water. The solubility also depends on the type of the side chain of the amino acid. Thus, compounds **2–4** bearing lipophilic side chains exhibit better solubility than **5** (with a more

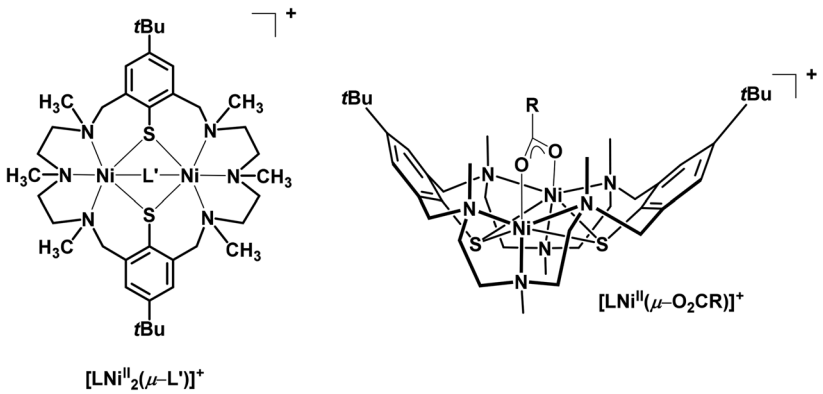

Fig. 1 Left: Chemical formula of dinuclear $[LNi_2(\mu\text{-}L')]^+$ complexes. Right: Perspective view of the structure of carboxylato-bridged $[LNi_2(\mu\text{-}O_2CR)]^+$ complexes.

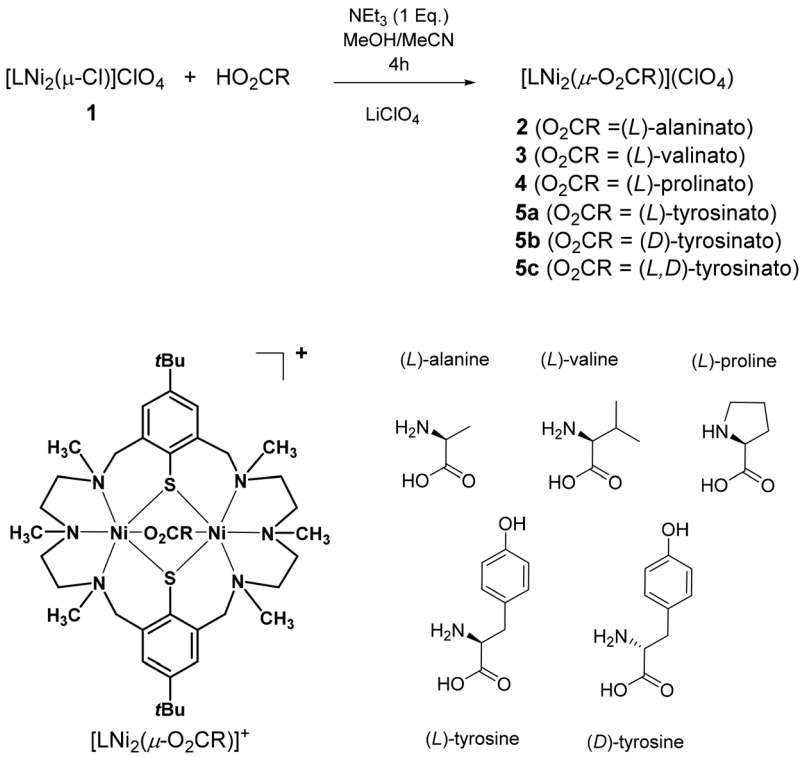

Scheme 2 Synthesis of compounds **2**–**5**. The corresponding tetraphenylborate salts **2′**–**5′** were obtained by salt metathesis with $NaBPh_4$.

Table 1 Selected analytical data for the perchlorate (**2**–**5**) and tetraphenylborate salts (**2′**–**5′**) of the $[LNi_2(\mu\text{-aminocarboxylato})]^+$ complexes

Compd	ESI-MS m/z	UV/Vis λ_{max}/nm	IR/cm^{-1} ν_{asym},ν_{sym} ($\Delta\nu$)	CD λ/nm ($\Delta\varepsilon$/M^{-1} cm^{-1})
2	872.4	648, 920, 1126[a]	1589, 1420 (169)	422 (+0.087), 633 (+0.050), 743 (+0.022)
2′	872.4	647, 920, 1123[a]	1586, 1421 (165)	424 (+0.067), 630 (+0.035), 756 (+0.012)
Alanine[36]			1592, 1408 (184)	
3	900.4	648, 921, 1092[a]	1588, 1419 (169)	415 (+0.114), 632 (+0.054), 731 (+0.034)
3′	900.5	649, 923, 1102[b]	1587, 1422 (165)	421 (+0.066), 629 (+0.045), 729 (+0.023)
Valine[36]			1575, 1424 (151)	
4	898.4	639, 918, 1088[a]	1625, 1421 (204)	413 (+0.004), 657 (+0.004)
4′	898.4	648, 921, 1098[b]	1625, 1422 (203)	412 (+0.010), 672 (+0.007)
Proline[37]			1619, 1402 (217)	
5a	964.4	647, 921, 1127[b]	1593, 1420 (173)	415 (+0.099), 633 (+0.059), 735 (+0.027)
5a′	964.4	646, 921, 1118[b]	1595, 1420 (175)	424 (+0.064), 628 (+0.040), 766 (+0.025)
L-Tyrosine[36]			1587, 1438 (149)	
5b	964.4	647, 921, 1127[b]	1592, 1418 (174)	423 (−0.102), 624 (−0.057), 746 (−0.032)
5b′	964.4	646, 921, 1118[b]	1595, 1422 (173)	424 (−0.069), 628 (−0.044), 766 (−0.023)
D-Tyrosine[36]			1587, 1438 (149)	
5c	964.4	647, 921, 1127[b]	1592, 1418 (174)	
5c′	964.4	646, 921, 1118[b]	1593, 1422 (171)	
DL-Tyrosine[36]			1587, 1439 (148)	

[a] MeOH–MeCN (1/2 v/v). [b] Solvent DMSO.

polar $-C_6H_4OH$ group) in MeCN, while the reverse is observed in MeOH.

Characterization of the aminocarboxylato complexes

The complexes were characterized by IR, UV/Vis, and circular dichroism (CD) spectroscopy to further ascertain the formulation of the products and to establish the coordination mode of the amino acids. The IR spectra show bands arising from the $[LNi_2]^{2+}$ fragment, the ClO_4^- or BPh_4^- counterions, and the amino carboxylato groups. Two prominent vibrations are seen in the IR,[38,39] as in other $\mu_{1,3}$-carboxylato-bridged Ni_2 complexes of $(L)^{2-}$,[40,41] around 1600–1580 cm^{-1} ($\nu_{asym}(RCO_2^-)$) and 1420–1400 cm^{-1} ($\nu_{sym}(RCO_2^-)$), indicating that the amino acids are also bound in this fashion. The IR absorptions of the

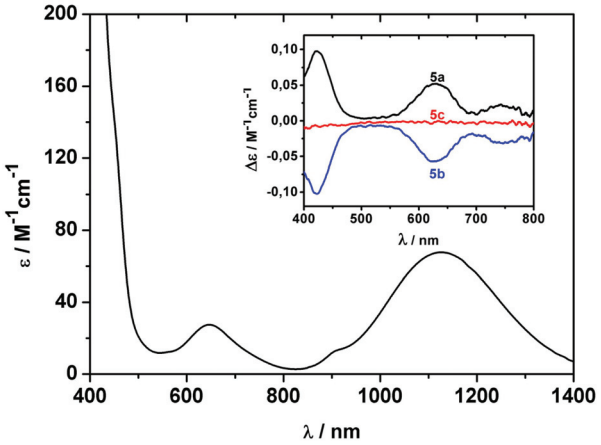

Fig. 2 UV/Vis spectrum of a 10^{-3} M solution of the L-tyrosinato complex **5a** in DMSO. Inset: CD-spectra of 10^{-3} M solutions of the L-tyrosinato, D-tyrosinato and L,D-tyrosinato complexes **5a–5c** in MeOH–MeCN (2/1) solution.

coordinated amino carboxylates are only slightly shifted relative to the corresponding values in their free, zwitterionic forms.[36,37,42] These frequency shifts are in good agreement with coordination of the carboxylate functions. The large separation of the two carboxylate stretching modes ($\Delta\nu = \nu_{asym} - \nu_{sym} > 160$ cm^{-1}) is also in line with a bridging mode.[38] The characteristic ν(NH) mode at 3300 cm^{-1} for the NH_3^+ group of free amino acids is absent in the complexes. The peaks at 3200 cm^{-1} correspond to the RNH_2 (or R_2NH (**4**)) groups.

Fig. 2 shows the UV/Vis spectrum of the tyrosinato complex **5a** which is representative for **2–5**. There are two weak absorption bands at 650 and 1100 nm attributable to the spin-allowed $^3A_{2g}\rightarrow{}^3T_{1g}$ (ν_2) and $^3A_{2g}\rightarrow{}^3T_{2g}$ (ν_1) transitions of a six-coordinate nickel(II) ion. The expected $^3A_{1g}\rightarrow{}^3T_{1g}$(P) transition (≤450 nm) is obscured by a strong $RS^-\rightarrow Ni^{II}$ charge transfer transition. The shoulder at approximately 920 nm can be attributed to a spin-forbidden $^3A_{2g}\rightarrow{}^1E_{1g}$(D) transition. Its observation implies a significant distortion from a pure octahedral coordination environment. Previous studies have shown that ν_1 and ν_2 are quite sensitive to the type of the bridging co-ligand.[28] For carboxylato complexes ν_1 = 1088–1028 nm and ν_2 = 648–655 nm),[28] very close to those of **2–5**. This match in values provides strong support for a $\mu_{1,3}$-bridging carboxylate function.

All compounds were further studied by CD spectroscopy. CD spectra were recorded from 400 to 800 nm in DMSO solution. The CD spectrum of the L-tyrosinato complex **5a** (inset to Fig. 2) is again representative for all compounds.

There are two positive peaks at 633 and 743 nm which presumably correspond to the ν_2 transition (at 650 nm), while the more intense peak at 422 nm is most likely a component of the ν_3 and/or the charge→transfer transition. The spectrum of the D-tyrosinato complex **5b** is similar to that of **5a**, but the three peaks have negative values as expected from the opposite configuration of the co-ligand. The racemate **5c** exhibits no net chirality, and its CD spectrum is featureless. There are not many examples in the literature to which the CD spectra of the present complexes can be compared. The spectra of octahedral [Ni(L-aminocarboxylato)$_2$(H_2O)$_2$] complexes have been reported.[43] Such compounds show two peaks for the ν_2 transition as well, but they have the opposite sign. This reversal of sign is presumably associated with the different coordination modes of the amino acids. The [Ni(L-aminocarboxylato)$_2$(H_2O)$_2$] complexes contain five-membered NO chelate rings. The puckering of the chelate rings confers dissymmetry about the metal ion and this effect contributes to the observed optical activity. In **2–5**, the CD spectra arise mainly from contributions from the asymmetric C atom, due to the absence of the NO chelate rings. Therefore, by simply looking at the sign of the CD peaks, one can readily indicate the presence of a *syn*,*syn*-bridged amino-carboxylato or a NO chelate structure.

Crystal structures of the prolinato (4′) and tyrosinato complex (5a)

Crystals of **4′**·2MeOH·MeCN suitable for single crystal X-ray diffraction analysis were grown from a methanol–acetonitrile solvent system. This salt crystallizes triclinic, space group *P*1. The crystal structure determination confirmed the presence of the carboxylato bridged [LNi_2(μ-L-prolinato)]$^+$ cation, BPh_4^- anions and MeOH and MeCN solvate molecules. There are two crystallographically independent but chemically identical [LNi_2(μ-L-prolinato)]$^+$ cations (molecule A and B) in the asymmetric unit. Fig. 3 shows the molecular structure of molecule A. Selected bond lengths and angles are given in the figure caption.

The $[LNi_2]^{2+}$ unit adopts a conical "calixarene-like" conformation typical for carboxylato-bridged Ni^{II} complexes of $(L)^{2-}$.

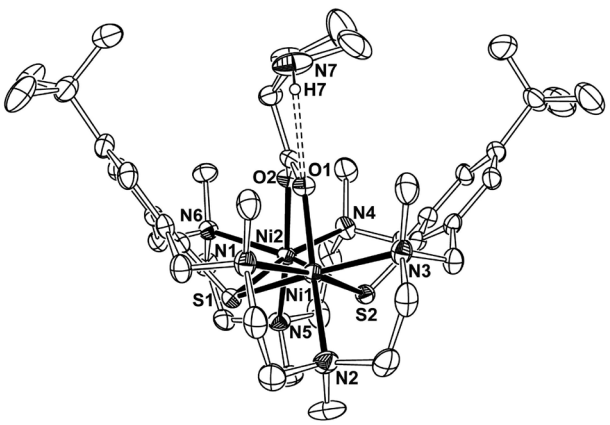

Fig. 3 Structure of the [LNi_2(μ-L-prolinato]$^+$ cation (molecule A) in crystals of **4**(BPh_4)·2MeOH·MeCN. Thermal ellipsoids are drawn at the 50% probability level. Hydrogen atoms have been omitted for clarity, except for the NH group. Selected bond lengths/Å (values in square brackets refer to molecule B): Ni1–O1 2.009(3) [2.019(2)], Ni1–N1 2.309(3) [2.266(3)], Ni1–N2 2.145(3) [2.148(3)], Ni1–N3 2.250(4) [2.251(3)], Ni1–S1 2.4791(13) [2.5063(16)], Ni1–S2 2.4463(14) [2.4395(12)], Ni2–O2 2.026(3) [2.011(3)], Ni2–N4 2.254(3) [2.234(3)], Ni2–N5 2.142(3) [2.160(4)], Ni2–N6 2.273(3) [2.287(3)], Ni2–S1 2.4857(13) [2.4967(13)], Ni2–S2 2.4613(14) [2.4309(12)]; N7···O1 = 2.752 [2.748] Å.

The nickel(II) ions are coordinated in a square-pyramidal fashion by a *fac*-$N_3(\mu\text{-}S)_2$ donor set. The prolinato ligand exhibits L-configuration and bridges the two six-coordinate Ni^{II} atoms in a symmetric fashion, at a Ni···Ni distance of 3.479(1) [3.477(1)] Å. The coordination environment of the nickel atoms is distorted octahedral, as manifested by large deviations from the ideal bond angles. The maximum deviation from the ideal angles is as large as 15.5(1)° (observed for the O(2)–Ni(2)–N(5) angle). The average Ni–N and Ni–S bond distances are 2.230(3) [2.224(3)] and 2.489(1) [2.468(1)] Å, respectively. Such bond lengths are common for bioctahedral Ni(II) complexes supported by $(L)^{2-}$.[25] The average Ni–O bond lengths are at 2.013(2) [2.016(3)] Å. Similar values are observed in other carboxylato-bridged $[LNi_2(\mu\text{-}O_2CR)]^+$ complexes indicating that the amino acids bind equally well to the dinuclear $[LNi_2]^{2+}$ fragment.

The crystal structure of the L-tyrosinato complex **5a** was characterized by X-ray crystallography using crystals of **5a**·2.25MeCN. The crystal structure comprises dinuclear $[LNi_2(\mu\text{-L-tyrosinato})]^+$ cations, perchlorate anions, and acetonitrile solvate molecules. There are two crystallographically independent $[LNi_2(\mu\text{-L-tyrosinato})]^+$ cations in the asymmetric unit, which differ slightly structurally as detailed below. The tyrosinato-complex (Fig. 4) is isostructural with the prolinato complex, with the tyrosinato ligand being coordinated in a bidentate bridging mode and the supporting ligand adopting the bowl-shaped "cone" conformation. Each cation is also connected to a ClO_4^- anion by an intermolecular hydrogen bond involving the phenolic OH group of the tyrosinato ligand (not shown in Fig. 4).

As mentioned above there are two $[LNi_2(\mu\text{-L-tyrosinato})]^+$ cations in the asymmetric unit, and their structures differ slightly. In molecule "A" the NH_2 group and the $CH_2C_6H_4OH$ side chain are located on different sides of the plane through the carboxylato group. In molecule "B" the two groups are on the same side of the carboxylato plane (the $CHNH_2CH_2C_6H_4OH$ group is rotated counter-clockwise by ~45° about the O_2C–$CHNH_2R$ bond). The occurrence of these two orientations can be traced to the presence of the intramolecular NH···O hydrogen bonding interactions involving the NH_2 and the carboxylato group (the NH_2 hydrogen atoms were located in the final Fourier map). The absence of the third possible orientation, in which the H and the $CH_2C_6H_4OH$ groups are on the same side of the carboxylato plane (and in which the NH_2 group is more remote from the O atoms thereby disfavouring the hydrogen bond) supports this assumption.

Synthesis of peptide complexes

The selective complexation of the amino acids prompted us to investigate the possible complexation of small peptides *via* their C-terminal carboxylate function. The three peptides (L-alanyl)$_n$-L-alanine (n = 1–3) were selected as they contain no side chains with potential donor atoms which would presumably interact with another $[LNi_2]^{2+}$ fragment. The reactions were performed in analogy to the synthesis of the amino carboxylate complexes above (Scheme 3). Thus, a suspension containing $[LNi_2(\mu\text{-Cl})](ClO_4)$ and the respective peptide was stirred in MeOH–MeCN in the presence of NEt_3 for 4 h to give a pale green solution, from which upon addition of an excess of $LiClO_4$ the corresponding $[LNi_2(\text{peptide})]^+$ complexes could be isolated as perchlorate salts **6–8** in 84–95% isolated yields. Salt metathesis of these with $NaBPh_4$ in MeOH furnished the corresponding tetraphenylborate salts **6′–8′**. The di-, tri-, and tetrapeptides react essentially in the same fashion as the amino carboxylates producing dinuclear mixed-ligand

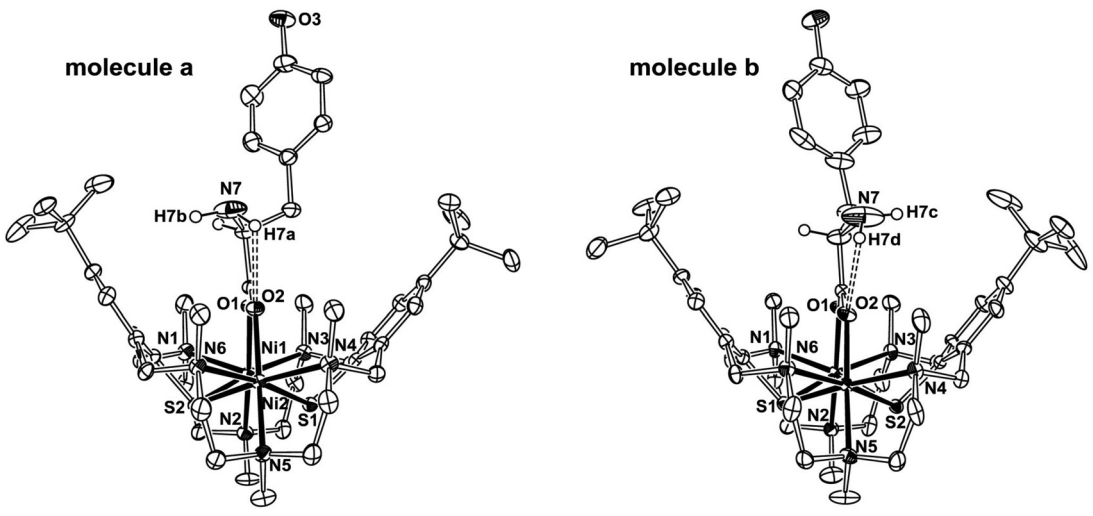

Fig. 4 Structure of the $[LNi_2(\mu\text{-L-tyrosinato}]^+$ cation (left molecule A, right molecule B) in crystals of **5a**·2.25MeCN. Thermal ellipsoids are drawn at the 50% probability level. Hydrogen atoms have been omitted for clarity, except for NH_2 groups. Selected bond lengths/Å (values in square brackets refer to molecule B): Ni1–O1 2.008(3) [2.014(3)], Ni1–N1 2.275(4) [2.270(3)], Ni1–N2 2.148(3) [2.140(3)], Ni1–N3 2.255(3) [2.260(3)], Ni1–S1 2.502(1) [2.467(1)], Ni1–S2 2.470(1) [2.486(1)], Ni2–O2 2.021(3) [1.999(3)], Ni2–N4 2.238(4) [2.260(3)], Ni2–N5 2.141(3) [2.137(3)], Ni2–N6 2.290(3) [2.240(4)], Ni2–S1 2.449(1) [2.487(1)], Ni2–S2 2.466(1) [2.467(1)]; N7a···O2a 2.742 Å, N7b···O2b 2.717.

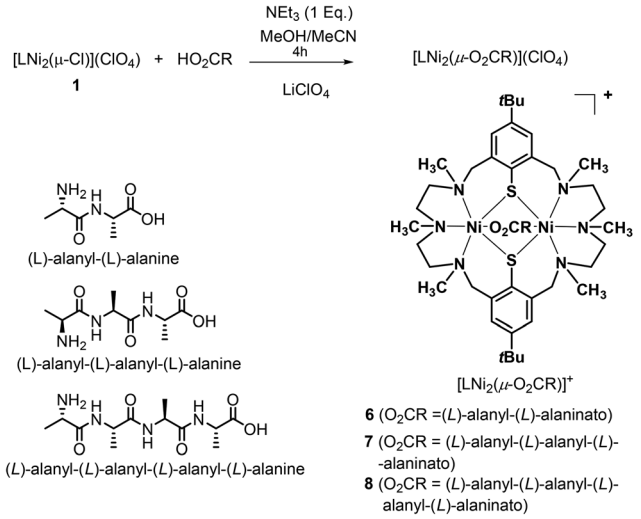

Scheme 3 Synthesis of the perchlorate salts **6–8**. The corresponding tetraphenylborate salts **6′–8′** were obtained by salt metathesis of **6–8** with $NaBPh_4$.

$[LNi_2(\mu\text{-peptide})]^+$ complexes with analogous structures in similar good yields and reaction times.

The perchlorate salts **6–8** are air stable in solution as well as in solid state. They exhibit good solubility in polar aprotic solvents such as MeCN, CH_2Cl_2 and acetone. They are less soluble in alcohol and virtually insoluble in water. Again, the solubility of compounds **6–8** was found to be dependent on the length of the peptide chain, similar to the side-chain dependence in case of the amino carboxylate complexes above. Thus, compound **8** is more soluble in methanol than **6**. In addition the complexes are more soluble than the free peptides. In MeOH–MeCN (2 : 1) the solubilities are 1.30×10^{-3} mol l^{-1} for (L-alanyl)-L-alanine, 0.65×10^{-3} mol l^{-1} for $(L\text{-alanyl})_2$-L-alanine, and 0.22×10^{-3} mol l^{-1} $(L\text{-alanyl})_3$-L-alanine. The perchlorate salts of the complexes are up to two orders of magnitude more soluble in the same solvent system (**6**: 5.83×10^{-3} mol l^{-1}, **7**: 7.33×10^{-3} mol l^{-1}, **8**: 16.08×10^{-3} mol l^{-1}). This is attributed to the partial encapsulation of the peptides in the binding pocket of $[LNi_2]^{2+}$ which hinders the formation of intermolecular hydrogen-bonding interaction which would otherwise lead to an extended network as present in the free peptides (Fig. 5).[44–47] It is assumed that part of the peptide chain is still exposed to the solvent medium, given that the binding pocket of the $[LNi_2]^{2+}$ unit has a depth of not more than ~6 Å. This would explain why the solubility increases with the length of the peptide chain.

Characterization of the peptide complexes

The peptide complexes were characterized by elemental analyses, ESI-MS, IR, UV/Vis and CD spectroscopy. Table 2 lists selected data.

The characterization data for the L-alanyl-L-alaninato complex **6** are representative. The electrospray ionization mass spectrum (ESI-MS) of a dilute methanol solution of **6** (ESI†) showed only two predominant peaks, corresponding to $[LNi_2(\mu\text{-L-alanyl-L-alaninato})]^+$ (m/z = 945.3) and $[LNi_2]^{2+}$ (m/z = 392.2), and the elemental analysis agreed well with the formulation of a 1 : 1 complex. The IR spectrum of **6** revealed two characteristic absorptions for a $\mu_{1,3}$-bridging carboxylate function at 1603 cm^{-1} ($\nu_{asym}(RCO_2^-)$) and 1417 cm^{-1} ($\nu_{sym}(RCO_2^-)$) (Fig. 6), as well as bands at 1100 and 625 cm^{-1} for the ClO_4^- ion. Another characteristic feature of the IR spectra is the amide I stretching mode,[48] associated mainly with the C=O group from the peptide backbone (Fig. 6). The frequency of this vibration is highly affected by structural changes associated to the loss or formation of hydrogen bonds which define the secondary structure of peptides.[49–52] A comparison of the IR spectra of L-alanyl-L-alanine and **6** shows that the amide I stretch is shifted by 23 cm^{-1} to lower energy, while for complexes **7** and **8** a hypsochromic shift by 27 and 35 cm^{-1} is observed. The shift to higher energy of the amide I vibration mode indicates a structural change which is believed to be a consequence of the encapsulation and the concomitant loss of intermolecular hydrogen bonds seen in the free peptides. The crystal structure of complex **6′** described below also supports this assumption.

The electronic absorption spectrum of **6** is very similar to that of **2** (Fig. 7), even the shoulder at 910 nm for the spin-forbidden $^3A_{2g} \rightarrow {}^1E_g(D)$ transition is observed, again indicative of a distorted octahedral $NiN_3S_2O^{carboxylato}$ chromophore in **6**. However, the spin-allowed $^3A_{2g} \rightarrow {}^3T_{1g}$ transition (a measure of the octahedral splitting parameter Δ_o)[53] at 1114 nm is slightly blue-shifted relative to **2** suggesting that the L-alanyl-L-alaninato ligand exerts a slightly stronger ligand field than the L-alaninato ligand. This may be traced to a weaker hydrogen-bonding interaction between the amide NH and the carboxylato-group, such that the latter is more basic in the dipeptide

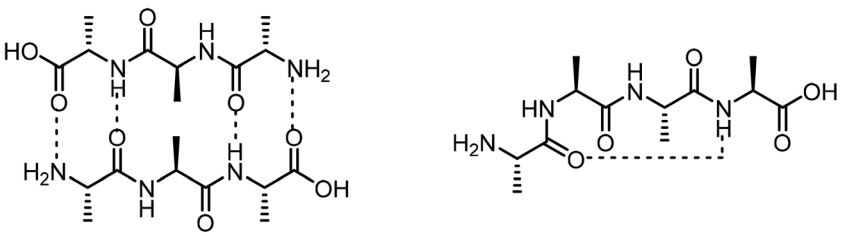

Fig. 5 Left: Intermolecular hydrogen bonding interactions in $(L\text{-alanyl})_2$-L-alanine leading to a β-sheet.[46] Right: α-Helix from intramolecular interaction in $(L\text{-alanyl})_3$-L-alanine.[47]

Table 2 Selected analytical data for the ClO_4^- and BPh_4^- salts of complexes **6–8**

Compd	ESI-MS m/z	UV/Vis λ_{max}/nm	IR, ν/cm^{-1} ν_{asym}, $\nu_s(RCO_2)$ ($\Delta\nu$);ν(CONH), δ(NH)	CD λ/nm ($\Delta\varepsilon$/M^{-1} cm^{-1})
6	943.3	648, 910, 1115[a]	1603, 1417 (186); 1662, 1507	421 (+0.060), 627 (+0.036), 756 (+0.013)
6′	943.3	649, 918, 1116	1602, 1420 (182); —, 1670	
(L-Alanyl)-L-Alanine[b]			1607, 1404 (203)	
			1685, 1560	
7	1014.4	650, 912, 1115[a]	1605, 1418 (187); 1676, 1489	421 (+0.065), 637 (+0.043), 762 (+0.051)
7′	1014.3	649, 918, 1113	1605, 1425 (180); 1676, 1483	
(L-Alanyl)$_2$-L-Alanine[b]			1595, 1428 (187)	
			1649, 1528	
8	1085.4	645, 909, 1106[a]	1605, 1418 (187); 1671, 1491	420 (+0.068), 633 (+0.052), 755 (+0.055)
8′	1085.4	640, 917, 1110	1607, 1424 (183); 1668, 1482	
(L-Alanyl)$_3$-L-Alanine[b]			1603, 1404 (199)	
			1633, 1540	

[a] MeCN. [b] IR (KBr).

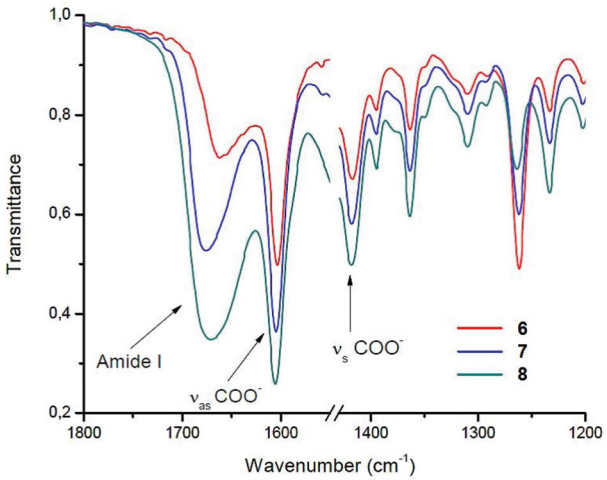

Fig. 6 IR spectra of compounds **6–8** (KBR pellets) in the 1800–1200 cm^{-1} region.

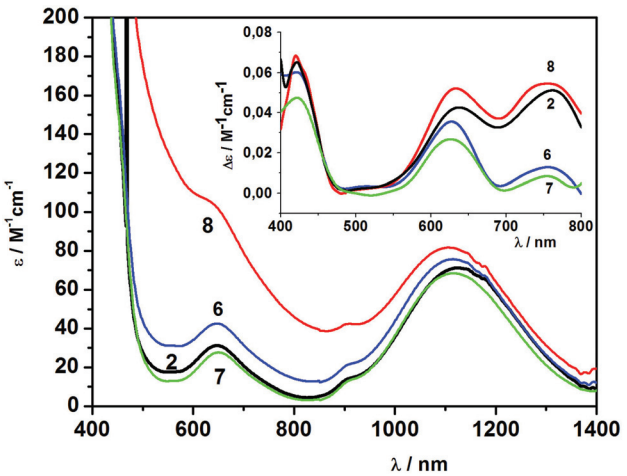

Fig. 7 UV/Vis and CD spectra (inset) of 10^{-3} M solutions of the perchlorate salts **6–8** in CH_3CN at room temperature.

and in turn the stronger ligand (the same applies to the tri and tetrapeptides in **7** and **8**, respectively). The $^3A_{1g}\rightarrow{}^3T_{2g}$ transitions appear to be not dependent on the type of the coligand, as they scatter randomly between 646 and 650 nm. The $^3A_{1g}\rightarrow{}^3T_{1g}(P)$ transition is again obscured by strong $RS^-\rightarrow Ni^{II}$ charge transfer transitions below 450 nm.

The inset to Fig. 7 shows the CD spectrum of **6**. Again, the spectrum is similar to that of **2** showing two positive peaks at 626 and 759 nm which correspond to the ν_2 transition (at 650 nm), and a peak at 418 nm assumed to be a component of the ν_3 (or the charge→transfer) transition. Overall, the spectroscopic similarities to the amino-carboxylato complexes provide strong support for a carboxylate-coordination of the peptide coligands.

Description of the crystal structure of the L-alanyl-L-alaninato complex 6′·2MeCN

We have not been able to grow single crystals of the tri- and tetrapeptide complexes **7** and **8** yet. However, in case of the L-alanyl-L-alaninato complex **6**, single crystals could be grown. The X-ray crystallographic analyses of the tetraphenylborate salt $[LNi_2(\mu\text{-L-alanyl-L-alaninato})]BPh_4\cdot 2MeCN$ (**6′**·2MeCN) unambiguously confirmed the presence of a $\mu_{1,3}$-bridging (L)-alanyl-L-alaninato coligand (Fig. 8). The asymmetric unit contains two crystallographically independent but chemically identical $[LNi_2(\mu\text{-L-alanyl-L-alaninato})]^+$ cations, two BPh_4^- anions and four acetonitrile solvate molecules. Besides the presence of the O,O-carboxylato coordination there are three significant structural differences from the free peptide:[44,45] (a) the absence of intermolecular H-bonding interaction of the L-alanyl-L-alaninato coligand, (b) the strong departure from a fully stretched peptide chain (*i.e.* the C43–N8 and the C42–N7 bonds are *cis* while they are *trans* in L-alanyl-L-alanine,[44,45] and (c) the presence of a bifurcated hydrogen bonding interaction of the amide NH donor with the carboxylato-O and the N-terminal NH_2 group. All these observations can be traced to the encapsulation of the dipeptide, which protects it from the surrounding medium. Such a protecting effect has not been observed previously for the $[LNi_2]^{2+}$ fragment. However, it is

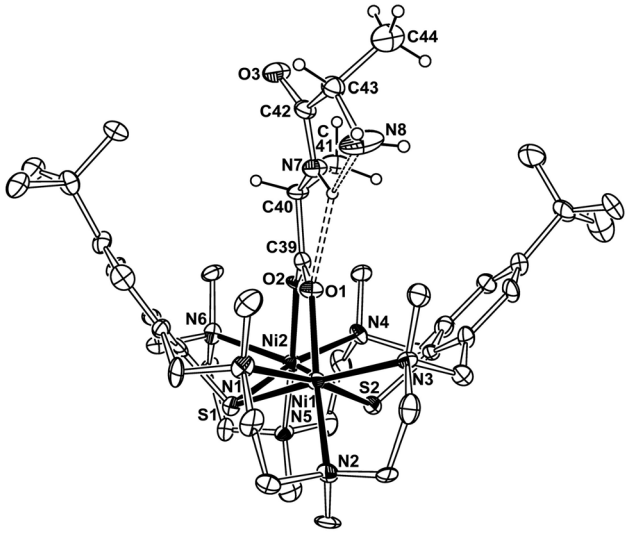

Fig. 8 Structure of the $[LNi_2(\mu\text{-L-alanyl-L-alaninato})]^+$ cation (molecule A) in crystals of **6′**·2MeCN. Thermal ellipsoids are drawn at the 50% probability level. Hydrogen atoms have been omitted for clarity, except for those of the peptide coligand. Selected bond lengths/Å (values in square brackets refer to molecule B): Ni1–O1 2.027(6) [2.015(7)], Ni1–N1 2.326(8) [2.301(7)], Ni1–N2 2.182(8) [2.136(8)], Ni1–N3 2.258(7) [2.283(9)], Ni1–S1 2.504(3) [2.492(3)], Ni1–S2 2.460(3) [2.494(3)], Ni2–O2 2.006(5) [2.010(7)], Ni2–N4 2.306(7) [2.320(8)], Ni2–N5 2.160(7) [2.146(8)], Ni2–N6 2.262(7) [2.280(8)], Ni2–S1 2.505(3) [2.490(3)], Ni2–S2 2.480(3) [2.471(3)]; N7···N8 2.766 [2.638], N7···O3 2.250 [2.279].

known that confinement in the binding pocket can lead to unusual conformations of the coligand. The other structural features in **6′** are normal. The average Ni–N, Ni–S and Ni–O bond lengths are at 2.247(8), 2.487(3), and 2.015(6) Å, respectively. The Ni···Ni distance is 3.496(1) [3.499(1)] Å in **6**. Virtually the same values are seen in **4a** and **5**.

Conclusion

Seven new macrocyclic complexes of the type $[LNi_2(\mu\text{-}O_2CR)]^+$ containing the anions of various α-aminoacids and oligopeptides as coligands were synthesized by reacting $[LNi_2(\mu\text{-Cl})]\text{-}ClO_4$ (**1**) with the corresponding coligand in methanol solution, namely $[LNi_2(\mu\text{-L-alaninato})]^+$ (**2**), $[LNi_2(\mu\text{-L-valinato})]^+$ (**3**), $[LNi_2(\mu\text{-L-prolinato})]^+$ (**4**), $[LNi_2(\mu\text{-L-tyrosinato})]^+$ (**5a**), $[LNi_2(\mu\text{-D-tyrosinato})]^+$ (**5b**), $[LNi_2(\mu\text{-L,D-tyrosinato})]^+$ (**5c**), $[LNi_2(\mu\text{-L-alanyl-L-alaninato})]^+$ (**6**), $[LNi_2(\mu\text{-(L-alanyl)}_2\text{-L-alaninato})]^+$ (**7**), and $[LNi_2(\mu\text{-(L-alanyl)}_3\text{-L-alaninato})]^+$ (**8**). The reaction yields appear to be not dependent on the chain length of the aminoacids or peptide. The complexes differ from other amino carboxylato structures in that they are selectively bound *via* their carboxylate groups and not as NO chelates. From IR spectra there is evidence about structural changes along the peptide backbone upon coordination to the dinuclear complex fragment. This fact is supported by the crystal structure of complex **6′** which reveals three major structural differences between the bound and the free dipeptide coligand. The solubility of the complexed oligopeptides is also altered upon coordination, which can be traced to the loss of intermolecular hydrogen bonding interactions upon encapsulation. The CD spectra of the *syn*, *syn*-bridged structures are significantly different from those of the NO chelates, and can distinguish between the two coordination modes. These results can now be used as a guide for the complexation of other oligopeptides.

Experimental section

General methods and instrumentation

IR spectra were recorded on a Bruker TENSOR 27 FT-IR-spectrometer. Electronic absorption spectra were recorded on a JASCO V670 UV/vis/NIR spectrometer. Elemental analyzes were carried out with a VARIO EL elemental analyzer. Compounds were dried under high vacuum for eight hours. Circular dichroism spectra were recorded on a JASCO J-715 spectropolarimeter. Mass spectra were taken on a BRUKER ESQUIRE 3000 PLUS instrument. Solvents and reagent were used in reagent purity. Amino acids from Alfa Aesar (D-, D/L-, L-tyrosine) and Sigma Aldrich (L-alanine, L-proline, L-valine) were optically pure and used without further purification. The syntheses of the metal complexes were carried out under a protective atmosphere of argon using standard Schlenk techniques. Starting Materials. Complex $[LNi_2(\mu\text{-Cl})](ClO_4)$ (**1**) was prepared according to the literature procedure.[40] All other reagents were obtained from standard commercial sources and used without further purification.

Safety Note! Perchlorate complexes are potentially explosive, and caution should be exercised when such derivatives are handled. However, the small quantities used in this study were not found to present a hazard. In our laboratory, small quantities of perchlorate complexes are routinely tested for their explosive potential by controlled mechanical impact.[54]

General procedure for the preparation of the carboxylato-bridged nickel(II) complexes **2–5**. Perchlorate salts: $[LNi_2(\mu\text{-L′})]\text{-}(ClO_4)$. To a solution of the chlorido-bridged complex **1** (92 mg, 0.10 mmol) in MeOH–MeCN (2 : 1) (30 mL) was added a suspension of the amino acid HL′ (0.10 mmol) in 5 mL of same solvent system, followed by 14 μL (0.10 mmol) of triethylamine. The mixture was stirred for 4 h to give a green solution. A solution of $LiClO_4{\cdot}3H_2O$ (0.16 g, 1.00 mmol) in EtOH (5 mL) was added. The solution was concentrated by evaporation at 40 °C to a volume of about 5 mL until incipient precipitation, and was then allowed to stand for another 6 h. The crude product was filtered, purified by recrystallization from a mixed MeCN–EtOH (1 : 1) solvent system, and dried under high vacuum for eight hours. Tetraphenylborate salts: The tetraphenylborate salts $[LNi_2(\mu\text{-L′})](BPh_4)$ were obtained as green powders by adding a solution of $NaBPh_4$ (342 mg, 1.00 mmol) in EtOH (5 mL) to a solution of $[LNi_2(\mu\text{-L′})](ClO_4)$ (0.10 mmol) in MeOH–MeCN (2 : 1) (30 mL). The crude product was filtered, purified by recrystallization from a mixed MeCN–EtOH (1 : 1) solvent system, and dried *in vacuo*.

Characterization data. [LNi_2(μ-L-alaninato)](ClO_4) (2). Yield: 87 mg (89 μmol, 91%). IR (KBr): ν/cm^{-1} = 2962 s, 2893 sh, 2868 s, 2806 m, 1589 s ($\nu_{as}(RCO_2^-)$), 1459 vs, 1420 m ($\nu_{symm}(RCO_2^-)$), 1170 w, 1153 m, 1097 vs, 1080 vs, 1061 s, 1041 s, 931 m, 752 w, 625 s. UV/Vis (MeOH–MeCN 2 : 1): λ_{max}/nm (ε/M^{-1} cm^{-1}) = 648 (20), 920sh, 1126 (58). MS (ESI+): *m*/*z* = 872.4 ([M − ClO_4]$^+$, 83%). Elemental analysis for $C_{41}H_{70}ClN_7Ni_2O_6S_2$ (974.01); C 50.11 (calc. 50.56), H 7.30 (7.24), N 9.79 (10.07) %.

[LNi_2(μ-L-alaninato)](BPh_4) (2′). Yield: 82 mg (69 μmol, 69%). IR (KBr), ν/cm^{-1}: 3033 m, 2963 s, 2867 s, 1586 s ($\nu_{as}(RCO_2^-)$), 1460 vs, 1421 m ($\nu_{symm}(RCO_2^-)$), 733 s, 704 vs, 627 w, 612 s. UV/Vis (MeOH–MeCN 2 : 1): λ_{max}/nm (ε/M^{-1} cm^{-1}): 647 (24), 920sh, 1123 (62). MS (ESI+): *m*/*z* = 872.4 ([M − BPh_4]$^+$, 90%). Elemental analysis for $C_{65}H_{90}BN_7Ni_2O_2S_2{\cdot}H_2O$ (1193.78 + 18.02): C 64.35 (calc. 64.42), H 7.49 (7.65), N 8.05 (8.09).

[LNi_2(μ-L-valinato)](ClO_4) (3). Yield: 56 mg (56 μmol, 56%). IR (KBr), ν/cm^{-1}: 2964 s, 2871 s, 1588 s ($\nu_{as}(RCO_2^-)$), 1486 m, 1463 s, 1419 m ($\nu_{symm}(RCO_2^-)$), 1379 w, 1363 m, 1151 m, 1102 vs, 1039 vs, 930 w, 754 w, 626 s. UV/Vis (MeOH–MeCN 2 : 1): λ_{max}/nm (ε/M^{-1} cm^{-1}) = 648 (30), 921sh, 1092 (67). MS (ESI+): *m*/*z* = 900.4 ([M − ClO_4]$^+$, 92%). Elemental analysis for $C_{43}H_{75}ClN_7Ni_2O_6S_2{\cdot}HClO_4{\cdot}H_2O$ (1002.06 + 18.02): C 50.61 (calc. 50.63), H 7.41 (7.51), N 9.56 (9.61).

[LNi_2(μ-L-valinato)](BPh_4) (3′). Yield: 121 mg (99 μmol, 99%). IR(KBr): 3054 m, 3034 m, 2999 m, 2982 m, 2963 s, 2927 m, 2901 m, 2867 s, 1587 s ($\nu_{as}(RCO_2^-)$), 1579 m, 1479 s, 1459 vs, 1422 s ($\nu_{symm}(RCO_2^-)$), 1396 m, 1362 m, 748 m, 734 s, 705 vs, 628 m, 612 m. UV/Vis (DMSO): λ_{max}/nm (ε/M^{-1} cm^{-1}) = 454sh, 649 (24), 923sh, 1102 (57). MS (ESI+): *m*/*z* = 900.5 ([M − BPh_4]$^+$, 89%). Elemental analysis for $C_{67}H_{94}BN_7Ni_2O_2S_2$ (1221.84): C 65.79 (calc. 65.86), H 7.63 (7.75), N 7.93 (8.02).

[LNi_2(μ-L-prolinato)](ClO_4) (4). Yield: 94 mg (94 μmol, 94%). IR (KBr), ν/cm^{-1}: 2962 s, 2901 s, 2869 s, 2807 m, 1625 s ($\nu_{as}(RCO_2^-)$), 1462 s, 1421 m ($\nu_{symm}(RCO_2^-)$), 1396 m, 1363 m, 1153 m, 1100 vs, 1077 vs, 1038 s, 930 m, 754 w, 625 s. UV/Vis (MeOH–MeCN 2 : 1): λ_{max}/nm (ε/M^{-1} cm^{-1}) = 639 (58), 918sh, 1088 nm (79). MS (ESI+): *m*/*z* = 898.4 (M − ClO_4, 98%). Elemental analysis for $C_{43}H_{72}ClN_7Ni_2O_6S_2{\cdot}H_2O$ (1000.05 + 18.02): C 50.64 (calc. 50.73); H 7.21 (7.33); N 9.49 (9.63).

[LNi_2(μ-L-prolinato)](BPh_4) (4′). Yield: 121 mg (99 μmol, 99%). IR(KBr): 3056 m, 3034 m, 3014 m, 2999 m, 2984 s, 2963 s, 2930 m, 2899 m, 2877 m, 1625 s ($\nu_{as}(RCO_2^-)$), 1579 m, 1480 s, 1462 vs, 1450 vs, 1422 m ($\nu_{symm}(RCO_2^-)$), 1393 m, 1363 m, 753 s, 734 vs, 710 vs, 627 w, 612 s. UV/Vis (DMSO): λ_{max}/nm (ε/M^{-1} cm^{-1}) = 453sh, 648 (24), 921sh, 1098 nm (57). MS (ESI+): *m*/*z* = 898.4 (M^+ − BPh_4, 40%). Elemental analysis for $C_{67}H_{92}BN_7Ni_2O_2S_2$ (1219.82): C 65.79 (calc. 65.97), H 7.63 (7.60), N 7.93 (8.04).

[LNi_2(μ-L-tyrosinato)](ClO_4) (5a). Yield: 86 mg (81 μmol, 81%). IR (KBr), ν/cm^{-1}: 2960 s, 2899 s, 2869 s, 2807 m, 1593 s ($\nu_{as}(RCO_2^-)$), 1516 s, 1485 m, 1462 vs, 1420 s ($\nu_{symm}(RCO_2^-)$), 1395 m, 1363 m, 1171 w, 1152 m, 1102 vs, 1077 vs, 1058 vs, 1041 s, 930 m, 752 w, 627 m., 1462 s, 1420 m, 1396 m, 1363 m, 1153 m, 1100 vs, 1077 vs, 1038 s, 930 m, 754 w, 625 s. UV/Vis (DMSO): λ_{max}/nm (ε/M^{-1} cm^{-1}) = 647 (25), 921sh, 1127 (60). MS (ESI+): *m*/*z* = 964.4 (M^+ − ClO_4, 93%). Elemental analysis for $C_{47}H_{74}ClN_7Ni_2O_7S_2$ H_2O (1067.11 + 18.02): C 51.88 (calc. 52.07), H 6.91 (7.07), N 9.01 (9.04).

[LNi_2(μ-L-tyrosinato)](BPh_4) (5a′). Yield: 127 mg (99 μmol, 99%). IR (KBr): 3053 s, 3036 m, 2998 s, 2982 s, 2964 s, 2925 m, 2898 m, 2864 s, 2807 m, 2612 w, 1595 s ($\nu_{as}(RCO_2^-)$), 1585 m, 1476 s, 1459 s, 1420 m ($\nu_{symm}(RCO_2^-)$), 1392 m, 1363 m, 774 w, 737 s, 705 vs, 629 m, 610 m. UV/Vis (DMSO): λ_{max}/nm (ε/M^{-1} cm^{-1}) = 450sh, 646 (22), 921sh, 1118 nm (51). MS (ESI+): *m*/*z* = 964.3 (M^+ − ClO_4, 95%). Elemental analysis for $C_{67}H_{92}BN_7Ni_2O_2S_2$ (1285.88 + 18.02): C 65.28 (calc. 65.40), H 7.31 (7.42), N 7.40 (7.52).

[LNi_2(μ-D-tyrosinato)](ClO_4) (5b). Yield: 90 mg (84 μmol, 84%). IR (KBr), ν/cm^{-1}: 2960 s, 2899 s, 2869 s, 2807 m, 1592 s ($\nu_{as}(RCO_2^-)$), 1516 s, 1485 m, 1462 vs, 1418 m ($\nu_{symm}(RCO_2^-)$), 1395 m, 1363 m, 1171 w, 1152 m, 1102 vs, 1077 vs, 1058 vs, 1041 s, 930 m, 752 w, 627 m, 1462 s, 1420 m, 1396 m, 1363 m, 1153 m, 1100 vs, 1077 vs, 1038 s, 930 m, 754 w, 625 s. UV/Vis (DMSO): λ_{max}/nm (ε/M^{-1} cm^{-1}) = 647 (25), 921sh, 1127 nm (60). MS (ESI+): *m*/*z* = 964.4 (M^+ − ClO_4, 93%). Elemental analysis for $C_{47}H_{74}ClN_7Ni_2O_7S_2{\cdot}H_2O$ (1084.12): C 51.95 (calc. 52.07), H 6.97 (7.07), N 8.96 (9.04).

[LNi_2(μ-D-tyrosinato)](BPh_4) (5b′). Yield: 90 mg (90 μmol, 90%). IR (KBr): ν/cm^{-1} = 3053 s, 3036 m, 2998 s, 2982 s, 2964 s, 2925 m, 2898 m, 2864 s, 2807 m, 2612 w, 1593 s ($\nu_{as}(RCO_2^-)$), 1585 m, 1476 s, 1459 s, 1422 w ($\nu_{symm}(RCO_2^-)$), 1392 m, 1363 m, 774 w, 737 s, 705 vs, 629 m, 610 m. UV/Vis (DMSO: λ_{max}/nm (ε/M^{-1} cm^{-1}) = 450sh, 646 (22), 921sh, 1118 (51). MS (ESI+): *m*/*z* = 964.3 (M^+ − ClO_4, 95%). Elemental analysis for $C_{71}H_{94}BN_7Ni_2O_3S_2$ H_2O (1285.88 + 18.02): C 65.33 (calc. 65.40), H 7.36 (7.42), N 7.44 (7.52).

[LNi_2(μ-D/L-tyrosinato)](ClO_4) (5c). Yield: 62 mg (58 μmol, 58%). IR (KBr), ν/cm^{-1}: 2960 s, 2899 s, 2869 s, 2807 m, 1592 s ($\nu_{as}(RCO_2^-)$), 1516 s, 1485 m, 1462 vs, 1418 m ($\nu_{symm}(RCO_2^-)$), 1395 m, 1363 m, 1171 w, 1152 m, 1102 vs, 1077 vs, 1058 vs, 1041 s, 930 m, 752 w, 627 m., 1462 s, 1420 m, 1396 m, 1363 m, 1153 m, 1100 vs, 1077 vs, 1038 s, 930 m, 754 w, 625 s. UV/Vis (DMSO): λ_{max}/nm (ε/M^{-1} cm^{-1}) = 647 (25), 921sh, 1127 nm (60). MS (ESI+): *m*/*z* = 964.4 (M^+ − ClO_4, 93%). Elemental analysis for $C_{47}H_{74}ClN_7Ni_2O_7S_2{\cdot}H_2O$ (1084.12): C 51.92 (calc. 52.07), H 7.01 (7.07), N 8.98 (9.04).

[LNi(μ-D/L-tyrosinato)](BPh_4) (5c′). 105 mg (82 μmol, 82%). IR (KBr): 3053 s, 3036 m, 2998 s, 2982 s, 2964 s, 2925 m, 2898 m, 2864 s, 2807 m, 2612 w, 1593 s ($\nu_{as}(RCO_2^-)$), 1585 m, 1476 s, 1459 s, 1422 m (ν_{symm} (RCO_2^-)), 1392 m, 1363 m, 774 w, 737 s, 705 vs, 629 m, 610 m. UV/Vis (DMSO): λ_{max}/nm (ε/M^{-1} cm^{-1}) = 450sh, 646 (22), 921sh, 1118 nm (51). MS (ESI+): *m*/*z* = 964.3 (M^+ − ClO_4, 95%). Elemental analysis for $C_{71}H_{94}BN_7Ni_2O_3S_2{\cdot}H_2O$ (1285.88 + 18.02): C 65.32 (calc. 65.40), H 7.37 (7.42), N 7.43 (7.52).

[LNi_2(μ-L-alanyl-L-alaninato)](ClO_4) (6). Yield: 99 mg (95 μmol, 95%). IR (KBr): ν/cm^{-1}: 2963, 2902, 2869 s (ν(C–H)), 1662 m (ν(C═O, amide I)), 1603 vs ($\nu_{as}(RCO_2^-)$), 1507 m (δ(N–H, amide II)), 1458 vs ($\delta_{sciss}(CH_2)/\delta(CH_3)$), 1417 m ($\nu_s(RCO_2^-)$), 1097 vs b ($\nu$(Cl–O)), 623 m ($\delta(ClO_4^-)$). UV-Vis (MeCN): λ_{max}/nm

(ε/M^{-1} cm^{-1}) = 646 (45), 910sh, 1114 (70). MS (ESI+): m/z = 943.4 (M^+ − ClO_4, 98%). Elemental analysis for $C_{44}H_{75}ClN_8Ni_2O_7S_2{\cdot}4H_2O$ (1045.09 + 72.06): C 47.14 (calc. 47.31), H 7.40 (7.49), N 10.30 (10.03), S 5.44 (5.74).

[LNi$_2$(μ-L-alanyl-L-alaninato)][BPh$_4$] (6′). Yield: 99 mg (78 μmol, 78%). IR (KBr): ν/cm^{-1}: 3397 m (ν(N–H)), 3054 m, 3033 m (ν(C–H arom.)), 2963 s, 2868 s (ν(C–H aliph.)), 1670 s (ν(C═O amide I)), 1602 vs ($\nu_{asym}(CO_2^-)$), 1581 m (ν(C═C arom.)), 1458 vs (δ_{sciss} $(CH_2)/\delta(CH_3)$), 1420 m ($\nu_s(RCO_2^-)$), 733 s, 705 vs (BPh_4^-). UV-Vis (MeCN): λ_{max}/nm (ε/M^{-1} cm^{-1}) = 649 (29), 918 sh, 1116 (72). MS (ESI+): m/z = 943.3 (M^+ − BPh_4, 97%). Elemental analysis for $C_{68}H_{95}BN_8Ni_2O_3S_2{\cdot}EtOH_2$ (1264.86 + 92.14): C 63.76 (calc. 63.73), H 7.51 (7.95), N 8.42 (8.26).

[LNi$_2$(μ-L-alanyl-L-alanyl-L-alaninato)][ClO$_4$] (7). Yield: 103 mg (92 μmol, 92%). IR (KBr): ν/cm^{-1}: 3425 s (ν(O–H assoc.)), 2963 s, 2869 s (ν(C–H)), 1676 s (ν(C═O, amide I)), 1605 vs ($\nu_{as}(RCO_2^-)$), 1489 s (δ(N–H, amide II)), 1459 vs ($\delta_{sciss}(CH_2)/\delta(CH_3)$), 1418 m ($\nu_s$ (RCO_2^-), 1098 vs b (ν(Cl–O)), 624 m ($\delta(ClO_4^-)$). UV-Vis (MeCN): λ_{max}/nm (ε/M^{-1} cm^{-1}) = 650 (25), 910sh, 1115 (62). MS (ESI+): m/z = 1014.4 (M^+ − ClO_4, 96%). Elemental analysis for $C_{47}H_{80}ClN_9Ni_2O_8S_2(H_2O)_3$ (1116.17 + 54.03): C 48.28 (calc. 48.24), H 7.48 (7.41), N 9.64 (10.77), S 5.70 (5.48).

[LNi$_2$(μ-L-alanyl-L-alanyl-L-alaninato)][BPh$_4$] (7′). Yield: 103 mg (77 μmol, 77%). IR (KBr) ν/cm^{-1}: 3424 vs b (ν(O–H)), 3055 m, 3034 m (ν (C–H arom.)), 2964 s, 2869 s (ν(C–H aliph.)), 1676 s (ν(C═O amide I)), 1605 vs (ν_{as} (RCO_2^-)), 1581 m (ν(C═C arom.)), 1483 s (δ(N–H, amide II)), 1458 vs ($\delta_{sciss}(CH_2)/\delta(CH_3)$), 1425 m ($\nu$s (RCO_2^-)), 734 vs, 705 vs (BPh_4^-). UV-Vis (MeCN): λ_{max}/nm (ε/M^{-1} cm^{-1}) = 649 (31), 918 sh 1113 (72). MS (ESI+) m/z (MeCN): 1014.3 (M^+ − BPh_4, 98%). UV-Vis (MeCN): λ_{max}/nm (ε/M^{-1} cm^{-1}) = 640 (61), 917 sh, 1110 (72). Elemental analysis for $C_{71}H_{100}BN_9Ni_2O_4S_2{\cdot}2EtOH$ (1335.96 + 92.14): C 64.37 (calc. 63.08), H 7.57 (7.91), N 8.63 (8.83).

[LNi$_2$(μ-L-alanyl-L-alanyl-L-alanyl-L-alaninato)][ClO$_4$] (8). Yield: 100 mg (84 μmol, 84%); IR (KBr) ν/cm^{-1}: 3423 s (ν(N–H)), 2964 s, 2870 s (ν(C–H)), 1671 s (ν(C═O, amide I)), 1605 vs ($\nu_{as}(RCO_2^-)$), 1491 s (δ (N–H, amide II)), 1457 vs (δ_{sciss} $(CH_2)/\delta$ (CH_3)), 1418 m ($\nu_s(RCO_2^-)$), 1107 vs b (ν(Cl–O)), 625 m ($\delta(ClO_4^-)$). UV-Vis (MeCN): λ_{max}/nm (ε/M^{-1} cm^{-1}) = 645 sh, 909sh 1106 (76). MS (ESI): m/z (MeCN): 1085.4 (M^+ − ClO_4). Elemental analysis for $C_{50}H_{85}ClN_{10}Ni_2O_9S_2{\cdot}3H_2O$ (1187.25 + 54.05): C 48.41 (calc. 48.38), H 7.58 (7.39), N 10.88 (11.28), S 5.14 (5.17).

[LNi$_2$(μ-L-alanyl-L-alanyl-L-alanyl-L-alaninato)][BPh$_4$] (8′). Yield: 101 mg (72 μmol, 72%). IR (KBr) ν/cm^{-1}: 3416 s b (ν(O–H)), 3055 m, 3035 m (ν(C–H arom.)), 2965 s, 2869 s (ν(C–H aliph.)), 1668 s (ν(C═O amide I)), 1607 vs ($\nu_{as}(RCO_2^-)$), 1581 m (ν(C═C arom.)), 1482 s (δ(N–H, amide II)), 1458 vs (δ_{sciss} $(CH_2)/\delta$ (CH_3)), 1424 m ($\nu_s(RCO_2^-)$), 735 vs, 706 vs (BPh_4^-). MS (ESI+): m/z (MeCN): 1085.4 (M^+ − BPh_4, 95%). UV/Vis (MeCN): λ_{max}/nm (ε/M^{-1} cm^{-1}) = 640 (61.4), 917sh, 1110 (72.0). Elemental analysis for $C_{74}H_{105}BN_{10}Ni_2O_5S_2{\cdot}H_2O$ (1407.04 + 18.02): C 62.43 (calc. 62.37), H 7.68 (7.57), N 9.68 (9.83).

Crystallography

The data sets for **4′**·2MeOH·MeCN, **5a**·2.5MeCN and **6′**·2MeCN were collected using a Bruker SMART CCD diffractometer equipped with graphite monochromated Mo-Kα radiation (0.71073 Å). The data were processed with SAINT and corrected for absorption using SADABS.[55] Structures were solved by Direct Methods[56] and refined by full-matrix least-squares on the basis of all data against F^2 using SHELXL-97.[57] PLATON was used to search for higher symmetry.[58] Ortep3 was used for the artwork of the structures.[59] Unless otherwise noted the anisotropic thermal parameters of all non-hydrogen atoms were refined. H atoms were placed at calculated positions and refined as riding atoms with isotropic displacement parameters. All non-hydrogen atoms were refined anisotropically. CCDC 982688 (**4′**·2MeOH·MeCN), CCDC 982689 (**5a**·2.25MeCN) and CCDC 1011258 (**6′**·2MeCN) contain the supplementary crystallographic data for this paper.

Crystal data for 4′·2MeOH·MeCN. $C_{71}H_{103}BN_8Ni_2O_4S_2$, M = 1324.96 g mol^{-1}, triclinic space group $P1$, a = 15.245(3), b = 16.340(3), c = 16.867(3) Å, α = 116.77(3), β = 105.89(3), γ = 95.67 (3)°, V = 3485.2(11) $Å^3$, Z = 2 (two crystallographically independent but chemically identical molecules A and B in the asymmetric unit), D_c = 1.263 g cm^{-3}, μ = 0.653 mm^{-1}, 22 331 reflections collected, 18 759 unique (R_{int} = 0.0154). The MeOH and MeCN are heavily disordered, and the electron density associated to these molecules was removed from the structure (and the corresponding F_o) with the SQUEEZE procedure implemented in the PLATON program suite.[60] Final R_1 [$F^2 > 2\sigma(F^2)$] = 0.0347 (R_1 = 0.0419 before SQUEEZE), wR_2 (all data) = 0.1016, R_1 index based on 18 759 reflections with $I > 2\sigma(I)$ (refinement on F^2). Flack x = 0.033(8). The H atom bonded to the secondary N atom of the prolinato ligand was located from a final Fourier map but was not refined. One *tert*-butyl group was found to be disordered over two positions. A split atom model was applied using the SADI instructions implemented in SHELXL to account for this disorder (C36B-C38B/C36C-C38C). The site occupancies (0.26/0.74) were refined.

Crystal data for 5a·2.5MeCN. $C_{51.50}H_{80.75}ClN_{9.25}Ni_2O_7S_2$, M = 1158.49 g mol^{-1}, triclinic space group $P1$, a = 14.0485(4), b = 15.2778(4), c = 16.2737(3) Å, α = 113.857(2), β = 97.723(2), γ = 111.779(2)°, V = 2795.05(12) $Å^3$, Z = 2 (two crystallographically independent but chemically identical molecules A and B in the asymmetric unit), D_c = 1.377 g cm^{-3}, μ = 0.854 mm^{-1}, 48 198 reflections collected, 26 658 unique (R_{int} = 0.0375). Final R_1 [$F^2 > 2\sigma(F^2)$] = 0.0348, wR_2 (all data) = 0.0949, R_1 index based on 22 501 reflections with $I > 2\sigma(I)$ (refinement on F^2). Flack x = 0.039(9).

Crystal data for 6′·2MeCN. $C_{72}H_{101}BN_{10}Ni_2O_3S_2$, M = 1346.98 g mol^{-1}, triclinic space group $P1$, a = 14.872(3), b = 16.889(3), c = 17.068(3) Å, α = 97.83(3), β = 105.66(3), γ = 115.48 (3)°, V = 3566.0(12) $Å^3$, Z = 2 (two crystallographically independent but chemically identical molecules A and B in the asymmetric unit), D_c = 1.254 g cm^{-3}, μ = 0.639 mm^{-1}, 25 832 reflections collected, 23 850 unique (R_{int} = 0.0731). Final R_1

$[F^2 > 2\sigma(F^2)]$ = 0.0339, wR_2 (all data) = 0.0722, R_1 index based on 22 501 reflections with $I > 2\sigma(I)$ (refinement on F^2). Flack x = 0.005(15). All MeCN solvate molecules were refined isotropically.

Acknowledgements

We are grateful to Prof. Dr E.-M. Hey-Hawkins and Prof. Dr A.-B. Sickinger for providing facilities for X-ray crystallographic and CD spectroscopic measurements.

References

1 D. A. Cataldo, K. M. McFadden, T. R. Garland and R. E. Wildung, *Plant Physiol.*, 1988, **86**, 734–739.
2 U. Krämer, J. D. Cotterhowells, J. M. Charnock, A. J. M. Baker and J. A. C. Smith, *Nature*, 1996, **379**, 635–638.
3 S. Sagner, R. Kneer, G. Wanner, J. P. Cosson, B. Deus-Neumann and M. H. Zenk, *Phytochemistry*, 1998, **47**, 339–347.
4 J. P. Laussac and B. Sarkar, *Biochemistry*, 1984, **23**, 2832–2838.
5 J. D. Glennon and B. Sarkar, *Biochem. J.*, 1982, **203**, 15–23.
6 M. Klewpatinond, P. Davies, S. Bowen, D. R. Brown and J. H. Viles, *J. Biol. Chem.*, 2008, **283**, 1870–1881.
7 R. P. Bonomo, D. La Mendola, G. Pappalardo, E. Rizzarelli and I. Sóvágó, in *Recent Development in Bioinorganic Chemistry: Metal Complexes of Bioactive Molecules*, ed. M. Saviano, Transworld Research Network, India, 2006, pp. 133–160.
8 (*a*) H. Sigel and R. B. Martin, *Chem. Rev.*, 1982, **82**, 385–426; (*b*) R. B. Martin, Nickel Binding to Amino Acids and Peptides, in *Metal Ions in Biological Systems*, ed. A. Sigel and H. Sigel, vol. 23, 1988, pp. 123–164; (*c*) F. Meyer and H. Kozlowski, in *Comprehensive Coordination Chemistry II*, ed. J. A. McCleverty and T. J. Meyer, Elsevier, vol. 6, 2004, pp. 247–554; (*d*) T. Kowalik-Jankowska, H. Kozlowski, E. Farkas and I. Sóvágó, *Met. Ions Life Sci.*, 2007, **2**, 63–108.
9 (*a*) K. Severin, R. Bergs and W. Beck, *Angew. Chem., Int. Ed.*, 1998, **110**, 1722–1743, (*Angew. Chem. Int. Ed.*, 1998, **37**, 1634–1654); (*b*) D. R. van Staveren and N. Metzler-Nolte, *Chem. Rev.*, 2004, **104**, 5931–5985.
10 (*a*) J. E. Letter Jr. and John E. Baumann Jr., *J. Am. Chem. Soc.*, 1970, **92**, 437–442; (*b*) T. B. Freedmann, D. A. Young, M. R. Oboodi and L. A. Nafie, *J. Am. Chem. Soc.*, 1987, **109**, 1551–1559.
11 H. Irving and R. J. P. Williams, *Nature*, 1948, **162**, 746–747.
12 E. Farkas and I. Sovago, *Amino Acids, Pept., Proteins*, 2007, **36**, 287–345.
13 I. Sóvágó and K. Ősz, *Dalton Trans.*, 2006, 3841–3854.
14 Y. Shimazaki, M. Takani and O. Yamauchi, *Dalton Trans.*, 2009, 7854–7869.
15 D. K. Nayak, K. K. Halder, R. Baishya, T. Sen, P. Mitrac and M. C. Debnath, *Dalton Trans.*, 2013, **42**, 13565–13575.
16 N. Burford, M. D. Eelman, W. G. LeBlanc, T. S. Cameron and K. N. Robertson, *Chem. Commun.*, 2004, 332–333.
17 (*a*) I. Csöreg, P. Kierkegaard, J. Legendziewicz and E. Huskowska, *Acta Chem. Scand.*, 1987, **A41**, 453–460; (*b*) I. Csöreg, P. Kierkegaard, J. Legendziewicz and E. Huskowska, *Acta Chem. Scand.*, 1989, **A43**, 636–640; (*c*) Q. Jin, X. Wang, T. Jin and G. Xu, *Polyhedron*, 1994, **13**, 2957–2961.
18 J. J. Zhang, T. L. Sheng, S. Q. Xia, G. Leibeling, F. Meyer, S. M. Hu, R. B. Fu, S. C. Xiang and X. T. Wu, *Inorg. Chem.*, 2004, **43**, 5472–5478.
19 J. Frelek, A. Klimek and P. Ruskowska, *Curr. Org. Chem.*, 2003, **7**, 1081–1104.
20 I. R. Baird, B. R. Cameron and R. T. Skerlj, *Inorg. Chim. Acta*, 2003, **353**, 107–118.
21 H. Tsukube, M. Wada, S. Shinoda and H. Tamiaki, *Chem. Commun.*, 1999, 1007–1008.
22 B. Korybut-Daszkiewicz, J. Taraszewska, K. Zieba, A. Makal and K. Wozniak, *Eur. J. Inorg. Chem.*, 2004, 3335–3344.
23 F. Meyer and H. Kozlowski, *ChemInform*, 2004, **35**, 247–554.
24 J. Schapp, K. Haas, K. Sünkel and W. Beck, *Eur. J. Inorg. Chem.*, 2003, 3745.
25 V. Lozan, C. Loose, J. Kortus and B. Kersting, *Coord. Chem. Rev.*, 2009, **253**, 2244–2260.
26 C. D. Gutsche Calixarenes revisited, in *Monographs in Supramolecular Chemistry*, ed. J. F. Stoddart, Royal Society of Chemistry, Cambridge, 1998.
27 V. Lozan and B. Kersting, *Inorg. Chem.*, 2008, **47**, 5386–5393.
28 U. Lehmann, J. Klingele, V. Lozan, G. Steinfeld, M. H. Klingele, S. Käss, A. Rodenstein and B. Kersting, *Inorg. Chem.*, 2010, **49**, 11018–11029.
29 B. Kersting, in *Activating Unreactive Molecules – The Role of secondary Interactions*, ed. C. Bolm and F. E. Hahn, Wiley-VCH, Weinheim, 2009, ch. 1, pp. 1–17.
30 B. Kersting and U. Lehmann, *Adv. Inorg. Chem.*, 2009, **61**, 407–470, (ed. R. v. Eldik and C. D. Hubbard).
31 J. Lach, A. Jeremies, V. Lozan, C. Loose, T. Hahn, J. Kortus and B. Kersting, *Inorg. Chem.*, 2012, **51**, 12380–12388.
32 T. Glaser, Y. Journaux, G. Steinfeld, V. Lozan and B. Kersting, *Dalton Trans.*, 2006, 1738–1748.
33 J. Klingele, M. H. Klingele, O. Baars, V. Lozan, A. Buchholz, G. Leibeling, W. Plass, F. Meyer and B. Kersting, *Eur. J. Inorg. Chem.*, 2007, 5277–5285.
34 S. Käss and B. Kersting, *Eur. J. Inorg. Chem.*, 2012, 2389–2401.
35 S. Käss, T. Gregor and B. Kersting, *Angew. Chem.*, 2006, **118**, 107–110, (*Angew. Chem., Int. Ed.*, 2006, **45**, 101–104).
36 R. J. Koegel, J. P. Greenstein, M. Winitz, S. M. Birnbaum and R. A. McCallum, *J. Am. Chem. Soc.*, 1955, **77**, 5708–5720.
37 A. W. Herlinger and T. V. Long II, *J. Am. Chem. Soc.*, 1970, **92**, 6481–6486.

38 K. Nakamoto, *Infrared and Raman Spectra of Inorganic and Coordination Compounds*, Wiley, New York, 5th edn, 1997.
39 G. B. Deacon and R. J. Phillips, *Coord. Chem. Rev.*, 1980, **33**, 227–250.
40 B. Kersting, *Angew. Chem.*, 2001, **113**, 4110–4112, (*Angew. Chem., Int Ed.*, 2001, **40**, 3987–3990).
41 J. Hausmann, M. H. Klingele, V. Lozan, G. Steinfled, D. Siebert, Y. Journaux, J. J. Girerd and B. Kersting, *Chem. – Eur. J.*, 2004, **10**, 1716–1728.
42 A. R. Garcia, R. B. de Barros, J. P. Loureno and L. M. Ilharco, *J. Phys. Chem. A*, 2008, **112**, 8280–8287.
43 R. A. Haines and M. Reimer, *Inorg. Chem.*, 1973, **12**, 1482–1486.
44 R. J. Fletterick, C.-C. Tsai and R. E. Hughes, *J. Phys. Chem.*, 1971, **75**, 918–922.
45 Y. Tokuma, T. Ashida and M. Kakudo, *Acta Crystallogr., Sect. B: Struct. Crystallogr. Cryst. Chem.*, 1969, **25**, 1367–1374.
46 A. Hempel, N. Camerman and A. Camerman, *Biopolymers*, 1991, **31**, 187–192.
47 S. Krimm, *Biopolymers*, 1983, **22**, 217–225.
48 J. Bandekar, *Biochim. Biophys. Acta*, 1992, **1120**, 123–143.
49 (*a*) W. C. Reisdorf, Jr. and S. Krimm, *Biochem.*, 1996, **35**, 1383–1386; (*b*) L. Wang, C. T. Middleton, M. T. Zanni and J. L. Skinner, *J. Phys. Chem.*, 2011, **B115**, 3713–3724.
50 J. W. Brauner, C. Dugan and R. Mendelsohn, *J. Am. Chem. Soc.*, 2000, **122**, 677–683.
51 R. Schweitzer-Stenner, *Vib. Spectrosc.*, 2006, **42**, 98–117.
52 (*a*) J. Grdadolnik, S. G. Grdadolnik and F. Avbelj, *J. Phys. Chem. B*, 2008, **112**, 2712–2718; (*b*) N. G. Mirkin and S. Krimm, *J. Phys. Chem. A*, 2002, **106**, 3391–3394.
53 A. B. P. Lever, *Inorganic Electron Spectroscopy*, Elsevier Science, Amsterdam, 2nd edn, 1984.
54 M. J. MacLachlan, M. K. Park and L. K. Thompson, *Inorg. Chem.*, 1996, **35**, 5492–5499.
55 *SADABS, An empirical absorption correction program part ot the SAINTPlus NT version 5.10 package*, BRUKER AXS, Madison, WI, 1998.
56 G. M. Sheldrick, *Acta Crystallogr., Sect. A: Fundam. Crystallogr.*, 1990, **46**, 467–473.
57 G. M. Sheldrick, *SHELXL-97, Computer program for crystal structure refinement*, University of Göttingen, Göttingen, Germany, 1997.
58 A. L. Spek, *PLATON – A Multipurpose Crystallographic Tool*, Utrecht University, Utrecht, The Netherlands, 2000.
59 L. J. Farrugia, *J. Appl. Crystallogr.*, 1997, **30**, 565.
60 P. v. d. Sluis and A. L. Spek, *Acta Crystallogr., Sect. A: Fundam. Crystallogr.*, 1990, **46**, 194.